Journal of Alloys and Compounds 848 (2020) 156167

Contents lists available at ScienceDirect

Journal of Alloys and Compounds

journal homepage: http://www.elsevier.com/locate/jalcom

Adiabatic potential energy surface of the Jahn-Teller complexes in CaF_2:Ni^{2+} crystal determined from experiment on ultrasonic attenuation

M.N. Sarychev [a], W.A.L. Hosseny [a, b], A.S. Bondarevskaya [a], I.V. Zhevstovskikh [a, c], A.V. Egranov [d, e], O.S. Grunskiy [f], V.T. Surikov [g], N.S. Averkiev [h], V.V. Gudkov [a, i, *]

[a] Ural Federal University, Institute of Physics and Technology, Ekaterinburg, 620002, Russia
[b] Faculty of Science, Department of Physics, Benha University, Benha, 13511, Egypt
[c] M.N. Miheev Institute of Metal Physics, UB of the RAS, Ekaterinburg, 620137, Russia
[d] A.P. Vinogradov Institute of Geochemistry, SB of the RAS, Irkutsk, 664033, Russia
[e] Irkutsk State University, Faculty of Physics, Irkutsk, 664003, Russia
[f] St. Petersburg State University, X-ray Diffraction Centre, St. Petersburg, 199034, Russia
[g] Institute of Solid State Chemistry, UB of the RAS, Ekaterinburg, 620990, Russia
[h] A.F. Ioffe Physical Technical Institute of the RAS, St. Petersburg, 194021, Russia
[i] South Ural State University, Chelyabinsk, 454080, Russia

ARTICLE INFO

Article history:
Received 10 March 2020
Received in revised form
31 May 2020
Accepted 21 June 2020
Available online 28 July 2020

Keywords:
Insulators
Optical materials
Crystal growth
Acoustic properties
Point defects
Ultrasonics

ABSTRACT

In CaF_2 crystal doped with Ni^{2+} ions, attenuation of all the normal ultrasonic modes with the wave vector $\mathbf{k} \parallel \langle 110 \rangle$ were investigated at 14–161 MHz in the temperature region of 5–120 K. The observed peaks of relaxation origin were interpreted as manifestation of the Jahn-Teller effect subject to the $T_{1g} \otimes (e_g + t_{2g})$ problem. The experimental data made it possible to estimate the parameters of adiabatic potential energy surface: the Jahn-Teller stabilization energies, the linear and quadratic vibronic coupling constants, location of the saddle points and the global minima defined in the 5-dimensional space of symmetrized (tetragonal and trigonal) coordinates.

1. Introduction

Traditional methods of investigation of electronic structure, dynamics and local symmetry of crystals are optical spectroscopy, electron spin resonance (ESR) and pulse techniques using electron spin echo (ESE, ESEEM spectroscopy) [1–4]. The same can be said about investigation of the Jahn-Teller effect (JTE) [5,6] in doped crystals. Recent studies of substituted II-VI and III-V compounds by means of ultrasonic technique demonstrated its efficiency in obtaining important information about structure and properties of the Jahn-Teller (JT) complexes [7–10]. The experiment is organized so that a certain wave generates strain of the same symmetry as of possible active vibronic mode. As a result, the energy of ultrasonic wave is transmitted to the JT subsystem and additional channel of dissipation appears. Investigation with the use of different normal modes grants unique opportunity to indicate unambiguously the symmetry properties of the global minima of adiabatic potential energy surface (APES) of the JT complexes. For example, in cubic crystals, anomalies in velocity and attenuation coefficient of the c_{44} mode indicate trigonal symmetry, anomalies in the $(c_{11} - c_{12})/2$ mode reveal tetragonal symmetry, and anomalies in both the modes justify orthorhombic symmetry of the global minima of APES. Quantitative information about temperature dependences of velocity and attenuation coefficient makes it possible to estimate parameters of APES, including the JT stabilization energies, the linear and quadratic constants of vibronic coupling, position of the APES extrema points: global minima, barriers between them and

* Corresponding author. Ural Federal University, Institute of Physics and Technology, Ekaterinburg, 620002, Russia.
E-mail address: v.v.gudkov@urfu.ru (V.V. Gudkov).

https://doi.org/10.1016/j.jallcom.2020.156167
0925-8388/

their coordinates in the space of symmetrized coordinates $(Q_\vartheta, Q_\varepsilon, Q_\xi, Q_\eta, Q_\zeta)$, [7–10].

The first ultrasonic investigation of the JTE in doped crystal was done with the use of corundum Al_2O_3 with the Ni^{3+} substitution in octahedral coordination [11]. Most of the substituted II-VI and III-V crystals recently investigated by ultrasonic technique had zinc-blende [7–9] or hexagonal [10] structure and incorporated the JT centers in tetrahedral coordination. Crystals with fluorite structure have cubic coordination of the JT centers (see Fig. 1) and, to our best knowledge, only one representative of such crystals was studied in ultrasonic experiment yet (see Refs. [12] and references therein).

It was SrF_2:Cr^{2+} with the Cr^{2+} ground orbital triplet ${}^5T_{2g}(t_{2g}^2 e_g^2)$. The position of the Cr^{2+} ion in cubic coordination in the degenerate state ${}^5T_{2g}$ is unstable resulting in the $T_{2g}\otimes(e_g + t_{2g})$ JTE problem with APES defined in the 5-dimensional space of the tetragonal e_g and trigonal t_{2g} displacements [13]. In the linear approximation of the vibronic coupling, the dominant interaction with one of these modes, e_g or t_{2g}, results in the tetragonal or trigonal minima of the APES, respectively. Account of the quadratic vibronic coupling terms involves both trigonal and tetragonal modes resulting in orthorhombic minima [6,13,14].

In the present paper, we report the results of investigation of one more representative of 3*d* substituted fluorites, CaF_2:Ni^{2+}, and reconstruction of APES of the cubic JT complex $Ni^{2+}F_8^-$. Nickel-doped fluorites were studied in Ref. [15,16] but there were Ni^+ and Ni^{2+} ions produced with the help of x-ray irradiation at room temperature. The first was associated with $(NiF_4)^{3-}$ molecular ion subject to the JTE with big off-center Ni^+ displacement, the second occupies Ca position, has ground orbital singlet ${}^4A_{1g}$ in cubic coordination (see Ref. [15] and references therein) and, therefore, cannot manifest the JTE.

In our case, Ni^{2+} ion in cubic coordination has ground orbital triplet ${}^3T_{1g}(t_{2g}^4 e_g^4)$ (see Table 1 in Ref. [11]), so the APES as well should be defined in the five-dimensional space. The questions are:

Table 1
Isothermal contribution of the JT sub-system to the total elastic modulus in a fluorite-type crystal.

Symmetry of the global minima	$[(c_{11}-c_{12})/2]_{JT}^T$	$(c_{44})_{JT}^T$
tetragonal minima	$-\frac{2}{9}\frac{na_0^2F_E^2}{k_BT}$	0
trigonal minima	0	$-\frac{16}{27}\frac{na_0^2F_T^2}{k_BT}$
orthorhombic minima	$-\frac{1}{72}\frac{na_0^2F_E^2}{k_BT}$	$-\frac{4}{9}\frac{na_0^2F_T^2}{k_BT}$

what approximation, linear or quadratic, should be used for description of the APES, what type of symmetry do the global minima possess, what are the values of the external points of the APES and where are they located? To answer these questions, we have measured attenuation of ultrasonic waves at 14–161 MHz in the temperature region of 5 – 120 K. Peak of attenuation was observed for all the normal modes propagating along the <110> crystallographic axis: transverse $c_T = c_{44}$ and $c_E = (c_{11} - c_{12})/2$ modes and longitudinal mode $c_l = c_B + c_T + c_E/3$, where the subscripts T and E indicate the trigonal and tetragonal moduli, respectively, and the subscript B relates to the bulk (totally symmetric) modulus $c_B = (c_{11} + 2c_{12})/3$. The peak was interpreted as due to relaxation in the sub-system of the JT complexes subject to the $T_{1g}\otimes(e_g + t_{2g})$ JTE problem. Relaxational anomalies found in attenuation of both in c_T and c_E modes pointed out the orthorhombic symmetry of the global minima, therefore, calculations of the APES parameters were done in the quadratic approximation of vibronic Hamiltonian.

2. Material and method

Crystals of CaF_2 doped with nickel were grown from the melt by the Bridgman-Stockbarger method in a helium atmosphere in the A.P. Vinogradov Institute of Geochemistry. Before loading the

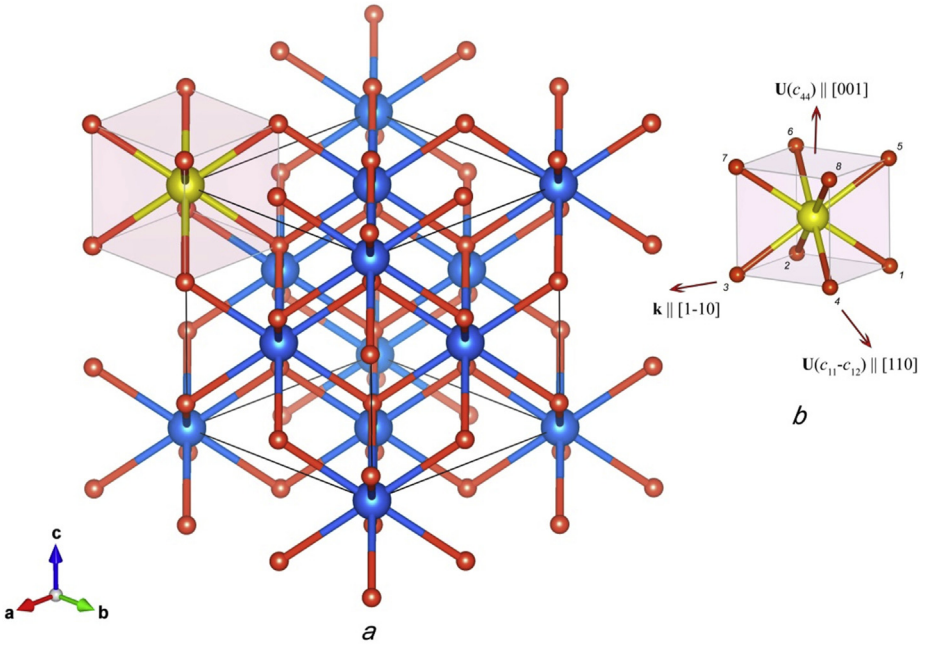

Fig. 1. Fluorite crystal structure (a) and cubic JT complex (b). Red are fluorine ions, blue are metal ions (Ca), yellow is Ni^{2+} substitution. **k** is the wave vector. It indicates the propagation direction of the ultrasonic mode. **U**(c_i) is the displacement produced by the wave associated with the elastic modulus $c_i = c_{44}$ or $(c_{11}-c_{12})/2$. (For interpretation of the references to colour in this figure legend, the reader is referred to the Web version of this article.)

mixture into the crucible, the salt of transition metal NiF_2 was dried in vacuum oven for several days. In the growth of alkaline earth fluorite single crystals, a small amount of CdF_2 is generally used as a scavenger in order to remove oxides and oxyfluorites contained in the raw materials by the reaction $CdF_2 + CaO \rightarrow CdO + CaF_2$. CdO and CdF_2 excess evaporate completely from the melt before crystallization begins. The samples were of high optical quality with no indication of oxygen contamination.

CaF_2 is a cubic crystal of the fluorite type structure $[Pm3m(O_h^3)]$ shown in Fig. 1 a. Its lattice parameter is $a = 5.462$ Å [17]. Ni ions substitute Ca and are surrounded by eight fluorine ions in the corners of the cube (see Fig. 1 b). Concentration of the dopand $n = (1.48 \pm 0.03) \times 10^{19}$ cm $^{-3}$ was determined at the Institute of Solid State Chemistry using an ELAN 9000 ICP-MS quadruple-based instrument (Perkin-Elmer SCIEX). It substantially exceeded the concentration of other 3*d* and 4*f* elements. The JT complexes can be considered as non-interacting due to large mean distance between the Ni^{2+} impurities.

Ultrasonic experiments were done at the Ural Federal University. Attenuation of the transverse and longitudinal ultrasonic waves was measured at 14–161 MHz. They were generated and detected by resonant $LiNbO_3$ piezoelectric transducers. The setup functioned as a frequency variable bridge. It had square-wave frequency and amplitude modulation and two phase detectors operating at the modulation frequency of 100 kHz. The outputs of the detectors were used as feedback signal for frequency bridge balance and for measuring the amplitude *u*. Description in detail can be found in Refs. [12]. The setup maintained the fixed phase regime. In this case, temperature variation of the attenuation coefficient $\Delta\alpha = \alpha(T) - \alpha(T_0)$ introduced as variation of the imaginary part of the complex wave number $k = \mathrm{Re}k - i\alpha$ is given (in neper per cm) as

$$\Delta\alpha = -\frac{1}{\ell}\ln\frac{u(T)}{u_0}, \tag{1}$$

where $u(T)$ is the voltage amplitude at the input of the receiver, $u_0 = u(T_0)$ is its reference magnitude, T_0 is the reference temperature, and ℓ is the distance covered by the ultrasonic wave.

Identification of the JTE problem can be done by means of analyzing the experimental data on ultrasonic attenuation of *E* and *T* symmetrized modes. Calculation of the isothermal contribution c_{JT}^T of the JT sub-system to the total elastic modulus *c* in the fluorite-type crystal for a triply degenerate orbital electronic state was given in Ref. [12] and is presented in Table 1 for the tetragonal and trigonal moduli. a_0 is the initial distance between the fluorine ions and the impurity (in our case it is Ni), k_B is the Boltzmann constant, F_E and F_T are tetragonal and trigonal vibronic coupling constants, respectively.

The relaxation origin attenuation of a normal mode (see, e.g., [18]) caused by the JT sub-system is proportional to the appropriate component of isothermal contribution to the total elastic modulus. In the dimensionless form, it is given as

$$\frac{(\alpha_{rel})_\beta}{k_{\beta 0}} = -\frac{1}{2}\frac{(c_\beta)_{JT}^T}{c_{\beta 0}}\frac{\omega\tau}{1+(\omega\tau)^2}, \tag{2}$$

where $(\alpha_{rel})_\beta$ is relaxational contribution to the total attenuation α_β , subscript β indicates the type of mode and associated modulus ($\beta = E, T, \ell$), ω is the cyclic frequency of the wave, τ is the relaxation time, $k_{\beta 0}$ and $c_{\beta 0}$ are the reference magnitudes (i.e., defined at $T = T_0$) of the wave number and the total elastic modulus, respectively. This expression describes the relaxational attenuation peak at approximately $\omega\tau = 1$. Hence, in accordance with Table 1, absence of attenuation peak for the trigonal mode justifies tetragonal symmetry of the global minima of APES (which takes place in the case of $T_{1g}\otimes e_g$ or linear $T_{1g}\otimes(e_g + t_{2g})$ JTE problem), absence of attenuation peak for the tetragonal mode points out trigonal symmetry of the global minima (the $T_{1g}\otimes t_{2g}$ or linear $T_{1g}\otimes(e_g + t_{2g})$ JTE problem), whereas observation of the peaks for both the modes evidences orthorhombic symmetry of the global minima (quadratic $T_{1g}\otimes(e_g + t_{2g})$ problem of the JTE). It should be mentioned that in the last case attenuation peak for the tetragonal mode should be much smaller in comparison with the peak for the trigonal mode (it is clearly seen in Table 1).

Eq. (2) indicates that relaxational attenuation vanishes both in adiabatic ($\omega\tau \gg 1$) and isothermal ($\omega\tau \ll 1$) regimes. Here we assume that temperature dependence of $1/\omega\tau$ is more strong than one proportional to *T*. Otherwise low temperature attenuation $\alpha_{rel} \propto 1/(k_B T\omega\tau)$ (according to Eq. (2) and Table 1) will exhibit increase approaching $T = 0$. We do not observe such increase. To obtain the relaxational contribution $(\alpha_{rel})_\beta$ from the total attenuation α_β which is measured in experiment, we will introduce α_β as the sum of relaxational $(\alpha_{rel})_\beta$ and the background attenuation $(\alpha_b)_\beta$ caused by all the other mechanisms. Fortunately, at the investigated temperatures, background attenuation can be approximated by monotonic function approaching the measured attenuation $\alpha_\beta(T)$ at low and high temperatures (i.e., at $T \ll T_1$ and $T \gg T_1$, where T_1 is the temperature corresponding to the condition $\omega\tau(T_1) = 1$ which approximately is the position of the attenuation peak in *T*-scale).

3. Results

As it was mentioned earlier, all the measured normal modes revealed peak which is well described by Eq. (2). The results of the experiment for longitudinal and two transverse modes are given in Fig. 2. Fig. 2a shows typical temperature shift of the relaxational peak caused by frequency reduction of the wave. Determination of the symmetry properties of the global minima can not be refer to an easy procedure. Traditional technique for this aid is EPR (see, e.g., Ref. [19–21]. It is based on the analysis of the angle dependence of the spectrum and actually reveals the symmetry of the static magnetic field in the position of paramagnetic ion. Ultrasonic experiment provides information about the dynamic elastic moduli. In the case of JTE manifestation, relaxation origin anomalies can be observed those are described by the isothermal contribution to the elastic modulus $(c_\beta)_{JT}^T$ (dependent on symmetry properties of the APES global minima) and relaxation rate τ^{-1} (dependent on the value of the potential energy barrier). Both of the methods are absolutely independent and should provide identic information about the JTE problem. Our experiments showed that the relaxation type anomaly (peak in temperature dependence of attenuation) is observed both in c_{44} and $(c_{11} - c_{12})/2$ modes. The explicit expressions of the isothermal moduli are given in Table 1. In case of tetragonal minima we would observe peak in the $(c_{11} - c_{12})/2$ mode and no anomaly in the c_{44} mode. In the case of trigonal minima, – vice versa. The case of peaks in both the modes relates to the orthorhombic type minima. On the basis of the experimental data, we can state that the minima of the APES have orthorhombic symmetry and, therefore, we should consider the quadratic $T_{1g}\otimes(e_g + t_{2g})$ JTE problem.

3.1. Relaxation time

Determination of the relaxation time from the experimental data requires (i) extraction of the relaxation attenuation caused by the JT subsystem $(\alpha_{rel})_\beta = \alpha_\beta - (\alpha_b)_\beta$ and (ii) calculation of the

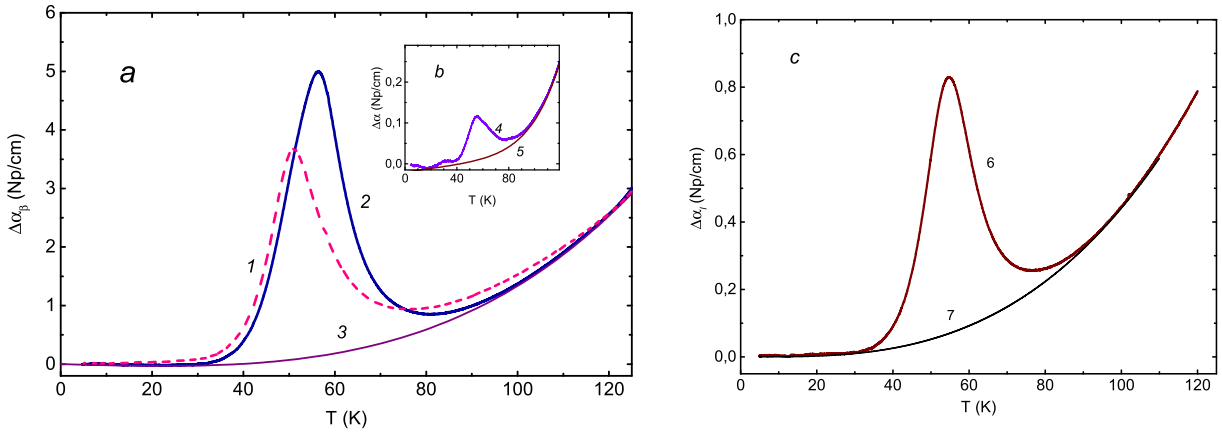

Fig. 2. Temperature dependences of ultrasonic attenuation: (a) *T*-mode c_{44} measured at 17 and 53 MHz (curves 1 and 2, respectively), (b) *E*-mode $(c_{11}-c_{12})/2$ at 54 MHz (curve 4). Background attenuation was defined as $(\alpha_b)_T = 4.32\times10^{-4} - 0.2\times10^{-3}\times T + 1.19\times10^{-6}\times T^3 + 3.45\times10^{-9}\times T^4$(curve 3), $(\alpha_b)_E = -0.02 + 4.2\times10^{-4}\times T + 2.19381\times10^{-8}\times T^3 + 10^{-11}\times T^4 + 1.1\times10^{-15}\times T^5 + 6.135\times10^{-14}\times T^6$ (curve 5), (c) longitudinal mode$c_l = c_B + c_T + c_E/3$ at 56 MHz (curve 6), and $(\alpha_b)_l = 10^{-3} - 10^{-4}\times T + 4.5\times10^{-6}\times T^3$ (curve 7).$\Delta\alpha_\beta = \alpha_\beta(T) - \alpha_\beta(T_0), T_0 = 5K$.

temperature dependence of the relaxation time using the following expression (see, e.g., Ref. [8]):

$$\tau(T) = \frac{1}{\omega}\left(\frac{\alpha_{rel}(T_1)\cdot T_1}{\alpha_{rel}(T)\cdot T} \pm \left[\left(\frac{\alpha_{rel}(T_1)\cdot T_1}{\alpha_{rel}(T)\cdot T}\right)^2 - 1\right]^{1/2}\right), \quad (3)$$

where T_1 corresponds to the condition $\omega\tau(T_1) = 1$. Sign (+) is taken for $T \le T_1$ and sign (−) is used for $T > T_1$. The subscript β in $(\alpha_{rel})_\beta$ is omitted in Eq. (3) for simplicity. The magnitude of T_1 can be obtained from the experimental data as the temperature corresponding to maximum of the curve $f(T) = \alpha_{rel}(T)\cdot T$. The temperature dependence of the relaxation time emerged from Eq. (3) is shown in Fig. 3. One can see that in the vicinity of attenuation peak (square symbol) relaxation time measured at transverse and longitudinal waves exhibits the dependence which is typical for activation mechanism $\tau_a \propto \exp V_0/k_B T$.

4. Discussion

In the case of quadratic $T\otimes(e+t_2)$ JTE problem, the E_E and E_T energies defines the depth of saddle points [6].

$$E_E = \frac{1}{2}\frac{F_E^2}{K_E}, \quad (4)$$

$$E_T = \frac{2}{3}\frac{F_T^2}{K_T}, \quad (5)$$

where K_E and K_T are primary force constants (i.e., evaluated without account of vibronic interaction). The orthorhombic minima lie below the lowest saddle point (calculations indicate it as E_T) by the magnitude of the energy barrier which approximately equals activation energy V_0 but more accurate calculation requires account of zero vibrations energy:

$$E_{OR} = E_T + V_0 + \frac{1}{2}\hbar\omega_R, \quad (6)$$

where ω_R is the radial vibronic frequency. Optical absorption spectra [22] indicated strong trigonal distortion of the JT complex in CaF_2:Ni^{2+} and CdF_2:Ni^{2+} crystals. EPR investigation of CdF_2:Ni^{2+} [22] revealed the trigonal vibrations as dominant with respect to the tetragonal ones, but it was outlined that coupling with the tetragonal vibrations cannot be neglected. Thus, the value of trigonal vibronic frequency 145 cm^{-1} (Table 12 in Refs. [22]) we assume as approximate value of ω_R. The force constant K_T is defined by the product of ω_τ^2 and the reduced mass of the NiF_8 complex $M = (m_{Ni}.8m_F)/(m_{Ni} + 8m_F)$. The force constants K_E and K_T describe elastic energy of the JT complex (in our case of E and T type) as a function of deformations given in the length units. Elastic moduli $(c_{11}-c_{12})/2$ and c_{44} describe the density of the free energy (its elastic part) of a crystal of the same symmetry but deformations are expressed in dimensionless form. From physical point of view the force constant and the elastic modulus of the same symmetry are native parameters. Since the primary force constants entering the expressions for the JT stabilization energy are defined without account of the JTE, we considered the relations between the force constants approximately equal to the relation between the elastic moduli of the same symmetry. In case of JT complex represents the unit cell, this relation should be absolutely correct. In our case, the JT complex is only a part of the unit cell, so the equality is approximate. In theoretical calculations K_E and K_T are assumed very often as equal. We considered that the assumption $(c_{11} - c_{12})/$

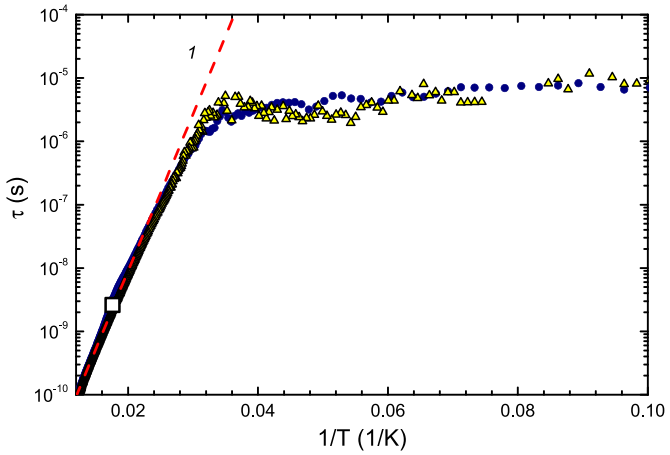

Fig. 3. Temperature dependence of relaxation time determined with the use of the data given in Fig. 2 (curves 2, 3, 6, and 7). Circles are experimental data obtained from the c_{44} mode at 54 MHz, triangles are experimental data obtained from the c_l mode at 56 MHz, and line 1 is activation relaxation time $\tau_a = 10^{-13}\exp(570/T)$. The square symbol indicates $\tau(T_1)$ for 54 MHz.

Table 2
Positions of six orthorhombic minima in coordinates $(Q_\vartheta, Q_\varepsilon, Q_\xi, Q_\eta, Q_\zeta)$.

	Q_ϑ	Q_ε	Q_ξ	Q_η	Q_ζ
Q_1^{OR}	$Q_{0\vartheta}^{OR}$	0	0	0	$Q_{0\zeta}^{OR}$
Q_2^{OR}	$Q_{0\vartheta}^{OR}$	0	0	0	$-Q_{0\zeta}^{OR}$
Q_3^{OR}	$-\frac{1}{2}Q_{0\vartheta}^{OR}$	$\frac{\sqrt{3}}{2}Q_{0\vartheta}^{OR}$	0	$Q_{0\zeta}^{OR}$	0
Q_4^{OR}	$-\frac{1}{2}Q_{0\vartheta}^{OR}$	$\frac{\sqrt{3}}{2}Q_{0\vartheta}^{OR}$	0	$-Q_{0\zeta}^{OR}$	0
Q_5^{OR}	$-\frac{1}{2}Q_{0\vartheta}^{OR}$	$-\frac{\sqrt{3}}{2}Q_{0\vartheta}^{OR}$	$Q_{0\zeta}^{OR}$	0	0
Q_6^{OR}	$-\frac{1}{2}Q_{0\vartheta}^{OR}$	$-\frac{\sqrt{3}}{2}Q_{0\vartheta}^{OR}$	$-Q_{0\zeta}^{OR}$	0	0

Table 3
Positions of three tetragonal saddle points in coordinates $(Q_\vartheta, Q_\varepsilon, Q_\xi, Q_\eta, Q_\zeta)$, where $Q_0^E = F_E/K_E$.

Q_1^E	Q_2^E	Q_3^E
$Q_0^E(1,0,0,0,0)$	$Q_0^E\left(-\frac{1}{2},\frac{\sqrt{3}}{2},0,0,0\right)$	$Q_0^E\left(-\frac{1}{2},-\frac{\sqrt{3}}{2},0,0,0\right)$

$2c_{44} \approx K_E/K_T$ is more reasonable than $K_E \approx K_T$. However, the advantage of such approach hardly can be estimated accurately. Thus,

$$K_T = \omega_\tau^2 M, \tag{7}$$

$$K_E = \frac{(c_{11}-c_{12})}{2c_{44}} K_T. \tag{8}$$

We have taken the following data for calculating the force constants: $c_{44} = 3.58 \times 10^{11}$ dyn/cm^2 and $(c_{11}-c_{12})/2 = 5.9 \times 10^{11}$ dyn/cm^2. As a result $K_T = 5.28 \times 10^4$ dyn/cm and $K_E = 8.71 \times 10^4$ dyn/cm. Positions of orthorhombic global minima can be calculated introducing the dimensionless parameters [14].

$$A = \frac{W_{ET}}{\sqrt{K_E K_T}}, \tag{9}$$

$$B = \frac{W_{ET} F_E}{K_E F_T}, \tag{10}$$

where W_{ET} is the quadratic vibronic coupling constant. Obviously,

$$W_{ET} = A\sqrt{K_E K_T}. \tag{11}$$

The values of A and B are defined by the equation

$$\frac{E_{OR}}{E_E} = \frac{(A/B)^2 - (A/B)A + 1/4}{\left(1-A^2\right)}, \tag{12}$$

The parameters A and B corresponding to global minima of orthorhombic symmetry are restricted by the areas bordered by

$$B = \left[-2A^2 \pm 2A\sqrt{3\left(1-A^2\right)}\right] \Big/ \left(3-4A^2\right), \quad B<0 \text{ or } B>1, \tag{13}$$

$$B = 2A^2 \pm \frac{2}{3}A\sqrt{3\left(1-A^2\right)}, \quad \sqrt{3} \Big/ 3-1 < B < 1. \tag{14}$$

Positions of the first orthorhombic minima is defined as follows

$$Q_1^{OR} = \left(-\frac{F_E\left(B-2A^2\right)}{2K_E B\left(1-A^2\right)}, 0, 0, 0, \left(-\frac{F_T(2-B)}{2K_T\left(1-A^2\right)}\right), \tag{15}$$

The other five can be obtained according to Table 2. Coordinates of the saddle points are given in Table 3 and 4

In the case of quadratic $T \otimes (e+t_2)$ JTE problem, the linear vibronic coupling constants can be calculated with the help of Eq. (2) written with the use of isothermal moduli listed in the last line of Table 1 and for the condition $\omega\tau = 1$ (i.e., for $T = T_1$) [12]:

$$F_E^2 = 288\frac{c_{E0}k_B T_1}{na_0^2}\frac{[\alpha_{rel}(T_1)]_E}{k_{E0}}, \tag{16}$$

$$F_T^2 = 9\frac{c_{T0}k_B T_1}{na_0^2}\frac{[\alpha_{rel}(T_1)]_T}{k_{T0}}, \tag{17}$$

where $a_0 = (\sqrt{3}/4)a = 2.36$ Å.

Typical error of attenuation measurements is 5%. The squared vibronic constants given by Eqs. (16) and (17) as well as stabilization energies [Eqs. (4)–(6)] are proportional to attenuation coefficient. The other variables entering these expressions are more accurate. Therefore, we can assume 5% as the error for evaluation of

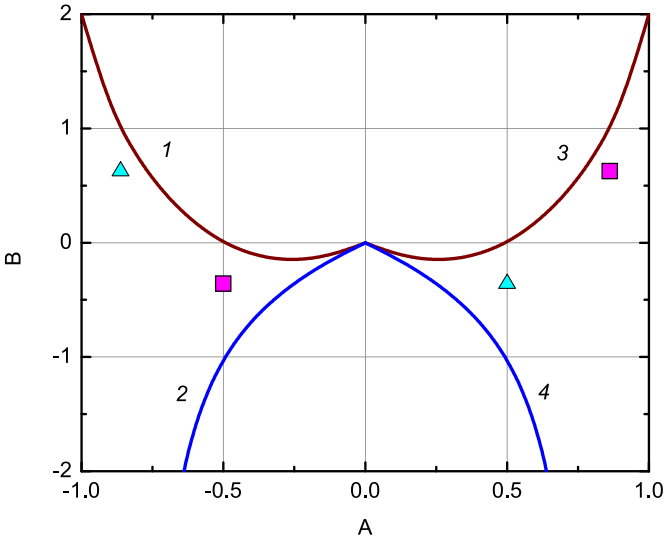

Fig. 4. Area of orthorhombic minima of the APES is restricted by the lines ($A = -1$, curves 1 and 2) and ($A = 1$, curves 3 and 4). Solutions of Eq. (14) for $A/B > 0$ are given by the square symbols and for $A/B < 0$ are the triangles.

Table 4
Positions of four trigonal saddle points in coordinates $(Q_\vartheta, Q_\varepsilon, Q_\xi, Q_\eta, Q_\zeta)$, where $Q_0^T = 2F_T/(3K_T)$.

Q_1^T	Q_2^T	Q_3^T	Q_4^T
$Q_0^T(0,0,1,1,1)$	$Q_0^T(0,0,-1,-1)$	$Q_0^T(0,0,1,-1,-1)$	$Q_0^T(0,0,-1,-1,1)$

Table 5
Parameters of the APES obtained from ultrasonic experiment for the cases $F_E, F_T > 0$ and $F_E > 0$, $F_T < 0$.

F_E, dyn	F_T, dyn	W_{ET}, dyn/cm	E_E, cm^{-1}	E_T, cm^{-1}	E_{OR}, cm^{-1}	Q_0^E, Å	Q_0^T, Å	$Q_{0\vartheta}^{OR}$, Å	$Q_{0\zeta}^{OR}$, Å
1.9×10^{-4}	$\pm 1.2 \times 10^{-4}$	$\mp 3.3 \times 10^4$, $\pm 5.9 \times 10^4$	350	880	1290	0.125	±0.15	− 0.20, 0.34	±0.35, ±0.59

the APES parameters.

Fig. 4 shows solutions of Eq. (12) for two cases: $A/B < 0$ and $A/B > 0$. All of them are located in the region of orthorhombic minima which is restricted by the areas ($A = -1$ and curves 1 and 2) and ($A = 1$ and curves 3 and 4). For $A/B > 0$ we have $A_1 = -0.49$, $B_1 = -0.36$ and $A_2 = 0.86$, $B_2 = 0.63$, while for $A/B < 0$ the parameters are $A_3 = -0.86$, $B_3 = 0.63$ and $A_4 = 0.49$, $B_4 = -0.36$. The results (A_1, B_1) and (A_4, B_4) seem to be more reliable with respect to (A_2, B_2) and (A_3, B_3) since they provide smaller values of $|W_{ET}| = 3.3 \times 10^4$ dyn/cm, $\left|Q_{0\vartheta}^{OR}\right| = 0.20$ Å and $\left|Q_{0\zeta}^{OR}\right| = 0.35$ Å (the last two pairs give $|W_{ET}| = 5.9 \times 10^4$ dyn/cm, $\left|Q_{0\vartheta}^{OR}\right| = 0.34$ Å and $\left|Q_{0\zeta}^{OR}\right| = 0.59$ Å).

The results of calculations based on the experimental data for (A_1, B_1) and (A_4, B_4) with the assumption $F_E > 0$ are given in Table 5.

5. Conclusions

In our investigation, we have studied manifestation of the JTE in the fluorite type crystal, CaF_2, doped with Ni^{2+} ions by means of ultrasonic technique. Temperature dependence of attenuation of all the normal ultrasonic modes propagating along crystallographic direction ⟨110⟩ were measured at 14–161 MHz in the region of 5–120 K. The observed peaks of relaxation origin were interpreted as due to relaxation in the sub-system of JT complexes $Ni^{2+}F_8^-$ subject to the $T_{1g} \otimes (e_g + t_{2g})$ JTE problem. Temperature dependence of relaxation time was constructed and activation energy was evaluated from this dependence. The relaxation peak of attenuation registered for all the investigated normal ultrasonic modes indicated the orthorhombic symmetry of the APES. The parameters of extrema points of the APES (minima and saddle points) were estimated. Namely, JT stabilization energies, the linear and quadratic vibronic coupling constants, and location of saddle points and global minima defined in the 5-dimensional space of symmetrized (tetragonal and trigonal) coordinates.

CRediT authorship contribution statement

M.N. Sarychev: Investigation, Project administration. **W.A.L. Hosseny:** Formal analysis. **A.S. Bondarevskaya:** Data curation. **I.V. Zhevstovskikh:** Validation, Writing - original draft. **A.V. Egranov:** Resources. **O.S. Grunskiy:** Resources. **V.T. Surikov:** Resources. **N.S. Averkiev:** Methodology, Writing - review & editing. **V.V. Gudkov:** Conceptualization, Supervision.

Declaration of competing interest

The authors declare that they have no known competing financial interests or personal relationships that could have appeared to influence the work reported in this paper.

Acknowledgements

In Ural Federal University this work was supported by the Russian Foundation for Basic Research (grant 18-32-00432 mol a), UrFU Center of Excellence “Radiation and Nuclear Technologies” (Competitiveness Enhancement Program), the Ministry of Education and Science of the Russian Federation (Program 5–100). In M.N. Miheev Institute of Metal Physics, this work was carried out within the state assignment of the Ministry of Education and Science of the Russian Federation (theme ``Electron" No. AAAA-A18-118020190098-5). In South Ural State University the work was partly supported by Act 211 Government of the Russian Federation, contract No 02.A03.21.0011. The technical support by the X-Ray Diffraction Resource Centre of Saint-Petersburg State University is gratefully acknowledged.

References

[1] M.M. Zaripov, V.F. Tarasov, V.A. Ulanov, G.S. Shakurov, M.L. Popov, Jahn-Teller ions of chromium in SrF_2 crystals: EPR studies in the range of 9.3-300 GHz, Phys. Solid State 37 (1995) 437.
[2] P.B. Oliete, V.M. Orera, P.J. Alonso, Continuous-wave and pulsed EPR studies of Cr^{2+} defects in CaF_2, Phys. Rev. B 53 (1996) 3047–3054, https://doi.org/10.1103/PhysRevB.53.3047.
[3] P.B. Oliete, V.M. Orera, P.J. Alonso, Structure of the Jahn-Teller distorted Cr^{2+} defect in SrF_2:Cr by electron-spin-echo envelope modulation, Phys. Rev. B 54 (1996) 12099–12108, https://doi.org/10.1103/PhysRevB.54.12099.
[4] S.K. Hoffmann, J. Goslar, S. Lijewski, V.A. Ulanov, Molecular structure and dynamics of off-center Cu^{2+} ions and strongly coupled $Cu^{2+} - Cu^{2+}$ pairs in BaF_2 crystals: electron paramagnetic resonance and electron spin relaxation studies, J. Chem. Phys. 127 (12) (2007) 124705, https://doi.org/10.1063/1.2768518.
[5] H.A. Jahn, E. Teller, Stability of polyatomic molecules in degenerate electronic states - I–orbital degeneracy, Proc. Roy. Soc. A 161 (1937) 220–235, https://doi.org/10.1098/rspa.1937.0142.
[6] I.B. Bersuker, The Jahn-Teller Effect, Cambridge University Press, 2006, https://doi.org/10.1017/CBO9780511524769.
[7] V.V. Gudkov, I.B. Bersuker, I.V. Zhevstovskikh, Y.V. Korostelin, A.I. Landman, Ultrasonic evaluation of the Jahn-Teller effect parameters. Application to ZnSe:Cr^{2+}, J. Phys. Condens. Matter 23 (11) (2011) 115401, https://doi.org/10.1088/0953-8984/23/11/115401.
[8] V.V. Gudkov, I.B. Bersuker, Experimental evaluation of the Jahn-Teller effect parameters by means of ultrasonic measurements. application to impurity centers in crystals, in: M. Atanasov, C. Daul, P.L. Tregenna-Piggott (Eds.), Vibronic Interactions and the Jahn-Teller Effect: Theory and Applications, Springer, Dordrecht, 2012, pp. 143–161, https://doi.org/10.1007/978-94-007-2384-9_7.
[9] N.S. Averkiev, I.B. Bersuker, V.V. Gudkov, K.A. Baryshnikov, I.V. Zhevstovskikh, V.Y. Mayakin, A.M. Monakhov, M.N. Sarychev, V.E. Sedov, V.T. Surikov, Ultrasonic investigation of the Jahn-Teller effect in GaAs semiconductors doped by transition metals, J. Appl. Phys. 116 (10) (2014) 103708, https://doi.org/10.1063/1.4895475.
[10] N.S. Averkiev, I.B. Bersuker, V.V. Gudkov, I.V. Zhevstovskikh, M.N. Sarychev, S. Zherlitsyn, S. Yasin, Y.V. Korostelin, V.T. Surikov, Ultrasonic determination of the Jahn–Teller effect parameters in impurity-containing crystals, J. Exp. Theor. Phys. 129 (1) (2019) 72–80, https://doi.org/10.1134/S1063776119060104.
[11] M.D. Sturge, The Jahn-Teller effect in solids, in: F. Seitz, D. Turnbull, H. Ehrenreich (Eds.), Solid State Physics, vol. 20, Academic Press, 1968, pp. 91–211, https://doi.org/10.1016/S0081-1947(08)60218-0.
[12] N.S. Averkiev, I.B. Bersuker, V.V. Gudkov, I.V. Zhevstovskikh, M.N. Sarychev, S. Zherllitsyn, S. Yasin, G.S. Shakurov, V.A. Ulanov, V.T. Surikov, The Jahn-Teller effect in elastic moduli of cubic crystals: general theory and application to strontium fluorite doped with chromium ions, in: M. van Asten (Ed.), Fluorite: Structure, Chemistry and Applications, Nova Science Publishers, New York, 2019, pp. 111–160. Ch. 2.
[13] I.B. Bersuker, V.Z. Polinger, Vibronic Interactions in Molecules and Crystals, Springer, Berlin, Heidelberg, 1989, https://doi.org/10.1007/978-3-642-83479-0.
[14] I.B. Bersuker, V.Z. Polinger, Jahn-Teller effect for T terms, Sov. Phys. JETP 39 (6) (1974) 1023–1029.
[15] J.C. Gonzalez, H.W. den Hartog, R. Alcala, EPR study of Ni_+ and Ni^{3+} in x-irradiated CaF_2, Phys. Rev. B 21 (1980) 3826–3832, https://doi.org/10.1103/PhysRevB.21.3826.
[16] J.A. Aramburu, P. García Fernández, M.T. Barriuso, M. Moreno, Big off-center displacements of ions in insulators: the Jahn-Teller ion Ni_+ in CaF_2, Phys. Rev. B 67 (2003), https://doi.org/10.1103/PhysRevB.67.020101, 020101.
[17] P. Eckerlin, H. Kandler, Structure Data of Elements and Intermetallic Phases,

Springer-Verlag, Berlin, Heidelberg, 1971, https://doi.org/10.1007/b19971.
[18] V.V. Gudkov, Ultrasonic consequences of the Jahn-Teller effect, in: H. Köppel, D.R. Yarkony, H. Barentzen (Eds.), The Jahn-Teller Effect: Fundamentals and Implications for Physics and Chemistry, Springer, Berlin, Heidelberg, 2009, pp. 743–766, https://doi.org/10.1007/978-3-642-03432-9_23.
[19] R. Fedder, Jahn-Teller distortions of Ag^{2+} ions in SrF_2 and CaF_2 by odd modes, Phys. Rev. B 2 (1) (1970) 32–39, https://doi.org/10.1103/PhysRevB.2.32.
[20] E.R. Zhiteitsev, V.A. Ulanov, M.M. Zaripov, E.P. Zheglov, EPR of trivalent iron centers in BaF_2:Fe crystal, Phys. Solid State 48 (10) (2006) 1779–1783, https://doi.org/10.1134/S1063783406100118.
[21] E.R. Zhiteitsev, V.A. Ulanov, M.M. Zaripov, EPR of trivalent iron centers in SrF_2: Fe crystals, Phys. Solid State 49 (5) (2007) 804–809, https://doi.org/10.1134/S1063783407050071.
[22] W. Gehlhoff, W. Ulrici, Transition metal ions in crystals with the fluorite structure, Phys. Status Solidi 102 (1) (1980) 11–59, https://doi.org/10.1002/pssb.2221020102.